Investigation of the directional Faraday cup and improvement of the comparison between direct and indirect thrust measurements of a magnetic nozzle ECR thruster

Romain Pioch, Victor Désangles, Pascal Chabert

RESEARCH ARTICLE | APRIL 30 2024

Investigation of the directional Faraday cup and improvement of the comparison between direct and indirect thrust measurements of a magnetic nozzle ECR thruster

Romain Pioch ; Victor Désangles ; Pascal Chabert

Phys. Plasmas 31, 043516 (2024)
https://doi.org/10.1063/5.0190318

Investigation of the directional Faraday cup and improvement of the comparison between direct and indirect thrust measurements of a magnetic nozzle ECR thruster

Cite as: Phys. Plasmas **31**, 043516 (2024); doi: 10.1063/5.0190318
Submitted: 5 December 2023 · Accepted: 4 April 2024 ·
Published Online: 30 April 2024

Romain Pioch,[1] Victor Désangles,[1,a)] and Pascal Chabert[2]

AFFILIATIONS

[1]Physics Instrumentation and Space Department, ONERA, Université Paris-Saclay, 91123 Palaiseau, France
[2]Laboratoire de Physique des Plasmas, CNRS, Ecole Polytechnique, Sorbonne Université, 91120 Palaiseau, France

[a)]**Author to whom correspondence should be addressed:** victor.desangles@onera.fr

ABSTRACT

The thrust of an electric propulsion device estimated from electrostatic probe measurements may be different from direct thrust measurements. In order to reduce this discrepancy for electron cyclotron resonance thrusters (ECRT), a new diagnostic is presented: the directional Faraday cup (FCDi). Thanks to a peculiar design, it assesses the angular distribution of ion current density in the plume of plasma thrusters. First, a theoretical model of the angular selectivity of the FCDi is introduced. It is validated with both simulations and experiments. Guidelines are given to use the FCDi in the plume of ECRT. Second, the observed discrepancies between direct thrust measurements made on a thrust stand and indirect ones are reduced when using the FCDi instead of a planar Faraday probe with a guard ring (FPGR). Relative errors come down to 10% with the FCDi, which are compared to 20%–30% observed with the FPGR. An analysis demonstrates that it is not due to the effect of local ion trajectories but comes from the magnitude of the ion current measured. A large sheath in front of the negatively biased FPGR seems to be the cause of this phenomenon. The grounded opening of the FCDi reduces this phenomenon and improves the ion flux measurement accuracy. This new probe, with angular selectivity characteristics, allows for the comparison of the ion flux ejection direction with the magnetic field line and contributes to a better description of ion population dynamic in the magnetic nozzle of the thruster.

I. INTRODUCTION

The rise of the new space industry in the last few decades has been accompanied by a reduction in spacecraft size and an evolution of their means of propulsion. For more than 30 years,[1] electric propulsion (EP) has been a serious alternative to the conventional chemical propulsion for station keeping or orbit raising missions. Despite generating less thrust force, it has the advantage of having a higher specific impulse and a greater overall efficiency, reducing significantly the mass of propellant necessary for a given mission. An EP system uses electrical power to generate a plasma and accelerate it at a high speed in order to produce a thrust force. Among the different types of EP systems that exist and constitute an active area of research, the most commonly used are the Hall effect thrusters (HET) and the gridded ion thrusters (GIT) but other devices also exist, either in flight or still in the prototype stage.[2] Among them, some use a diverging magnetic field to accelerate a plasma and produce thrust.[3–5] This is the case of the electron cyclotron resonance (ECR) thruster developed at Office National d'Études et de Recherches Aérospatiales (ONERA) and the object of the present study.

To compare EP systems and assess their performance, several quantities are commonly used.[6] The thrust is among the most important. However, other quantities and different thrust production efficiencies can also be evaluated. First, the specific impulse (ISP) accounts for the velocity of ejection of the accelerated particles. It is proportional to the ratio between the thrust and the propellant mass flow rate. Second, the mass efficiency is the ratio of ionized and, therefore, accelerated particles to the propellant mass flow rate injected, and is critical for long lasting missions. Third, when the electric power onboard the spacecraft is limited, the produced thrust to consumed electrical power ratio (TTPR) is central. Fourth, the divergence

efficiency accounts for the ratio of the thrust actually produced compared to the thrust that would be produced if all of the particles were ejected in the thrust direction. Therefore, the thrust is necessary to evaluate many of the performance indicators of EP devices. It is then crucial to measure it with great precision.

The direct way to measure the thrust of an EP device is to use a thrust balance, also referred to as a thrust stand. This diagnostic provides an integrated value of the produced thrust. One way to realize this measurement is to mount the thruster on a pendulum arm and measure the displacement of this arm when the thruster is firing. This diagnostic offers a calibrated measurement with a precision up to 0.1 μN.[7] However, it has the disadvantage of being complex and expansive to develop, bulky, and subject to environmental vibrations and perturbations in the lab. It can be used only in the laboratory and cannot be easily moved from one facility to another. Moreover, it is difficult to bring much electrical power or cooling fluids on the arm of a thrust balance without deteriorating its sensibility and accuracy.

The thrust of an EP device can also be indirectly estimated from the properties of the plasma ejected that are measured with electrostatic probes. More specifically, the thrust is estimated by integrating the local ion pressure on a close surface of the plume of the thruster (i.e., the plasma ejected by the thruster). To do so, one type of electrostatic probe, designed to measure the ion flux of EP devices and called Faraday probe, is used. It consists of an electrode facing the flux of charged particles which is biased at a voltage sufficiently low to repel the electrons and collect only the ions. The measured current flowing from the plasma to the probe divided by the collection surface area is called the ion current density. This quantity is typically measured at different positions in the plasma ejection region of an EP device by mounting the probe on translation or rotation stages. Together with the ion ejection velocity, measured either by an ion energy analyzer, a retarding potential analyzer, or by laser-induced fluorescence (LIF), it allows to compute the local pressure applied by the plasma and the thrust produced by the thruster. Contrary to thrust stands, the use of electrostatic diagnostics also gives access to key parameters of the operation of the thruster, such as the total ion current, the mass efficiency, or the divergence efficiency. However, unlike optical diagnostics, electrostatic diagnostics and Faraday probes are perturbative and a special care must be taken in their design and usage.[8] Recent studies showed that cup-shaped Faraday probes, called Faraday cups, seem more suited than planar probes to provide precise measurements of the ion current density.[9] In fact, they offer more control of the plasma sheath and their design allows the recollection of secondary electron emission (SEE), which are two of the main issues encountered when measuring the ion current density with the value of the plasma parameters involved in the context of low power EP. Active research concerning Faraday cup depth, shape, or material was conducted in recent years in the plume of field emission electric propulsion thrusters (FEEP) and HET in view of accuracy improvement and standardization of ion current measurements for EP systems.[10–16]

In the case of EP devices, such as HET, GIT, or FEEP thrusters, direct and indirect measurements of the thrust are in good agreement.[17] However, this comparison is not valid for the ECR thruster. In Ref. 18, the author recovered the thrust of a HET measured with a thrust balance thanks to measurements made with a Faraday probe with guard ring with a relative error below 5%, while more than 20% was observed for the ECR thruster under the same conditions. An assumption is that the non-local acceleration of the ions, in the diverging magnetic field of the magnetic nozzle, produces bent ion trajectories that are the source of the discrepancy observed. The investigation and reduction of this discrepancy would be of great interest in the understanding of plasma behavior in expansion in a magnetic nozzle. In order to tackle this problem and get rid of certain assumptions believed to be too restrictive in the estimation of the current density, a new diagnostic, the directional Faraday cup (FCDi), has been thought and designed.

This paper has two main objectives: to present and characterize the behavior of this new diagnostic in the plume of the ECR thruster and to give the elements necessary to understand why the Faraday probe with guard ring (FPGR) is not suited to the study of this EP device. It is organized as follows. To begin with, Sec. III presents the FCDi. A theoretical study is conducted and experimentally validated. Simulation results confirmed by experiments demonstrate that this probe allows meaningful measurements of the ion current density. In Sec. IV, the advantages of this new Faraday cup design over a classical design are justified with the comparison between direct and indirect thrust measurements of the ECR thruster over a wide range of operating conditions. Section V discusses the results obtained and gives insights on the overestimation of ion current density obtained with the FPGR. Eventually, Sec. VI concludes the paper and gives perspectives on the utilization of the FCDi in the study of the ion expansion in a magnetic nozzle.

II. EXPERIMENTAL APPARATUS

A. The B09 facility

Experiments have been conducted at ONERA in the B09 vacuum facility represented in Fig. 1. This vacuum tank is a cylinder of 80 cm in diameter and 2 m in length. The pressure inside the chamber can be brought down to a few 10^{-7} mbar with a pumping speed of 12 000 L · s^{-1}. These pumping capabilities are achieved by the combination of a roughing pump, three turbo-molecular pumps, and a cryogenic pump and are measured with a *MKS999 Quattro* vacuum transducer. When the ECR thruster is firing, the pressure inside the B09 is 1.1×10^{-6} mbar at 1 sccm of xenon mass flow rate and 1.7×10^{-6} mbar at 2.5 sccm. Inside the chamber, the ECR thruster is hung to a thrust balance specifically designed for this facility.[19]

The vessel is equipped with a rotation arm that allows to move a probe along an arc in front of the thruster with a precision under 0.1°. The location of the probe with respect to the thruster is then defined by a couple of values (ρ and θ), ρ being the distance to the thruster and θ the angle formed by the rotating arm and the axis of the thruster as pictured in Fig. 1.

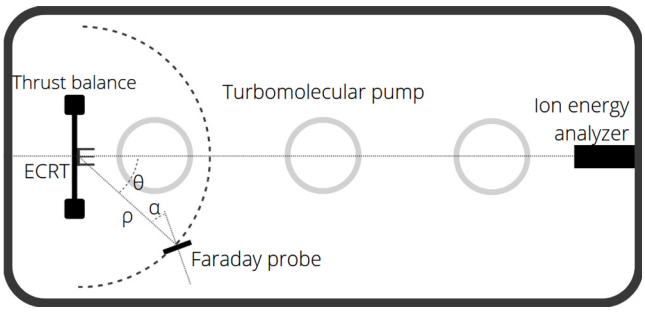

FIG. 1. Schematic cross section view of the B09 facility.

A *PSM003 ion analyzer* from *Hiden Analytical* is mounted on the port opposite to the thruster. This mass spectrometer measures the energy of the ions emitted by the thruster. The ion analyzer can be removed to replace it with the ion source mentioned later in the paper.

B. The ECR thruster

The electron cyclotron resonance (ECR) thruster (Fig. 2) is an EP device for satellites developed at ONERA. Among its advantages, this thruster has a very simple design and is electrodeless. A gas, mainly xenon, is introduced in a cylindrical cavity of 27 mm in diameter and 20 mm in length called the source, closed at one end by a dielectric piece called the backplate. Inside the source, an inner conductor of 2 mm in diameter has the role of an antenna. A 2.45 GHz microwave with a power around 30 W is fed through this coaxial chamber which is evenly filled with xenon at a controlled flow rate. Around the source, an annular permanent magnet generates a strong magnetic field that forms a diverging magnetic nozzle (MN) downstream the source. The value of the magnetic field near the backplate is chosen so that the cyclotron frequency of the electrons at this location matches the microwave frequency, creating a plasma by ECR heating. Electrons and ions expand and accelerate in the diverging MN before detaching from the magnetic field lines through processes that are beyond the scope of this paper. This is the ejection of the plasma at high velocity which is at the origin of the thrust of the device. Since 2010, the ECR thruster has been the object of much research at ONERA,[18,20–22] yielding an innovative design with high performances. Moreover, it gained maturity on several points: stability of operation, design robustness, or performance improvement.

C. Ion source

An ion source is used in this work to verify the acceptance angle of the directional Faraday cup (see Sec. III). It is mounted on the B09 facility to benefit from its pumping capabilities. This source is composed of a wire anode running through a cylindrical cavity (the cathode) filled with xenon at low pressure. A high voltage power supply imposes a voltage drop between the anode and the cathode, noted as V_d. It results in the generation of a plasma inside the cavity. Thanks to a second voltage supply, the whole device is floated at a positive voltage V_f with respect to the B09 vacuum tank tight to ground. A hole pierced in the cathode lets an ion beam flow out of the device inside the vacuum chamber. This beam is nearly mono energetic, with an energy peaked around $V_d + V_f$, because ions are produced near the anode. A preliminary work not presented in this paper has been carried out beforehand to characterize and control the ion source. It showed that the radius of the beam a few centimeters away from the source exit is between 0.75 and 1 cm depending on the ion energy and the divergence angle is below 10°. This is sufficiently low to consider the ion beam to be mono directional. A complete description of this device operation can be found in Ref. 23.

D. Faraday probe with guard ring

The Faraday probe available at the beginning of this work has been designed following the guidelines of Ref. 8. It is composed of a collector of diameter $d_c = 5.9$ mm and a guard ring of diameter $d_{GR} = 50$ mm, both made of molybdenum to reduce secondary electron emission. The gap between the collector and the guard ring is 100 μm, which is negligible compared to d_c and d_{GR}. The purpose of the guard ring is to flatten the sheath that forms in front of the probe when biased at high negative voltage so that the ion collection area in front of the collector remains a disk, therefore, limiting the overestimation of ion current density. The biasing voltage is −350 V for both the collector and the guard ring (see Sec. III C 1 for more details).

E. Data acquisition

Figure 3 represents the electrical circuit used to measure the ion current drawn by a Faraday probe while biasing it. Such a circuit is duplicated for every part of the probe that needs to be biased independently. The value of R_{shunt} is of a few tens of $k\Omega$ and needs to be adjusted to the current measured to protect the data acquisition system. Data are acquired thanks to a National Instrument PCIe 6323 acquisition card connected to a PC. For Faraday probe measurements, data points are acquired with a sampling rate of 939 Hz during 2 s and averaged overtime to increase the precision. The acquisition card is also used to output the control voltage fed to an *Applied Kilovolt HPZ series* power supply which biases the electrodes of the Faraday probes. Good care was taken to power this amplifier with external batteries to reduce noise and current leaks to the ground. The ECR thruster monitoring signals, such as source temperature and floating potential as well as thrust balance signals, are acquired continuously with a sampling rate of 40 Hz.

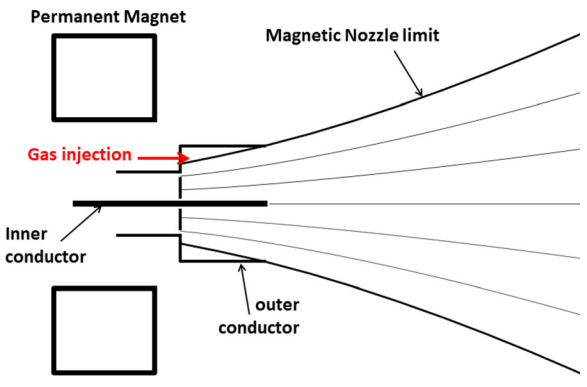

FIG. 2. The ECR thruster and the magnetic nozzle.

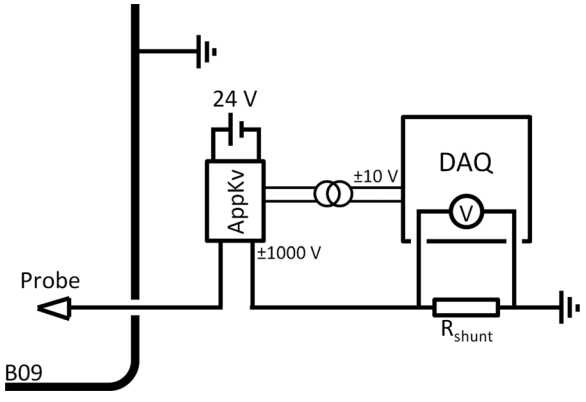

FIG. 3. Schematic drawing of biasing and acquisition of electrical circuit.

III. THE DIRECTIONAL FARADAY CUP

A. Probe description

The directional Faraday cup (FCDi) has been designed to capture the angular distribution of ion current density in the plume of EP devices. In fact, it collects only the particles whose trajectory make a small angle with the probe axis. With respect to the notations displayed in Fig. 4, the dimensions of the FCDi are $\ell = 34$, $r_p = 2.95$, and $r_o = 1.5$ mm. Its conception is based on a Faraday cup design. However, as pictured on the computer assisted design view in Fig. 4 and contrary to a classic Faraday cup, this diagnostic has the peculiarity of having two distinct collectors electrically disconnected from each other: the plate made of molybdenum and the cylinder made of graphite, that can be biased independently. Therefore, particles that hit those two collectors generate two distinct signals. The probe can then be used in two modes: the directional mode, for which the plate and collector signal are looked at independently, and the cup mode, for which the two signals are summed. Finally, a third piece placed at the probe entrance called the ring can also be biased, grounded, or left floating. Such a probe has been designed to be mounted on a small stepper motor. Thus, it can rotate around its own axis, adding a degree of freedom for ion current density measurements.

The angular selectivity of this probe is investigated in this section before its application to the indirect estimation of the thrust produced by an ECR thruster. To do so, the trajectory of ions impacting the probe is studied under two regimes: an ideal regime, where ions are not subject to electric fields, collisions, or sheath effects, and a plasma regime, where electric fields generated by the probe biasing and the sheath formation are taken into account. Several approaches will be used for each of these regimes and will be described, together with associated results, in the next two subsections.

B. Probe collection in the ideal regime

1. Theoretical definition of acceptance and opening functions

The directionality of a probe is quantified by its acceptance $\mathcal{A}$. This function is defined as the proportion of the plate area impacted by a rectilinear particle beam entering the probe at an angle β with respect to the probe axis, as pictured in Fig. 4. The opening area $\mathcal{O}$ is the proportion of cup (plate and cylinder) impacted by this beam. For a given geometry of the probe, the acceptance function depends on its opening radius r_o, its plate radius r_p, and its length ℓ. It is normalized by the area of the entrance hole of the probe so that $\mathcal{A}(\beta = 0) = 1$.

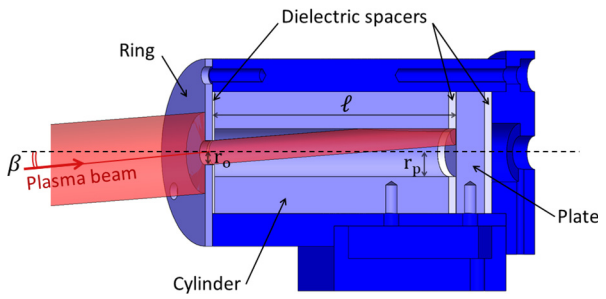

FIG. 4. Cross section view of the directional Faraday cup with a mono directional plasma beam.

Analytical forms for $\mathcal{A}$ and $\mathcal{O}$ can be found. When the probe rotates in front of an observer with an angle β, the ring and the plate observed are two ellipses separated by a distance $D = |\ell \sin(\beta)|$ with a semi-major axis r_o and r_p and a semi-minor axis $r_o \cos(\beta)$ and $r_p \cos(\beta)$, respectively. An approximation of the acceptance, called $\mathcal{A}'$, neglecting the thickness of the opening ring, is defined as the intersection area of those two ellipses as pictured in Fig. 5.

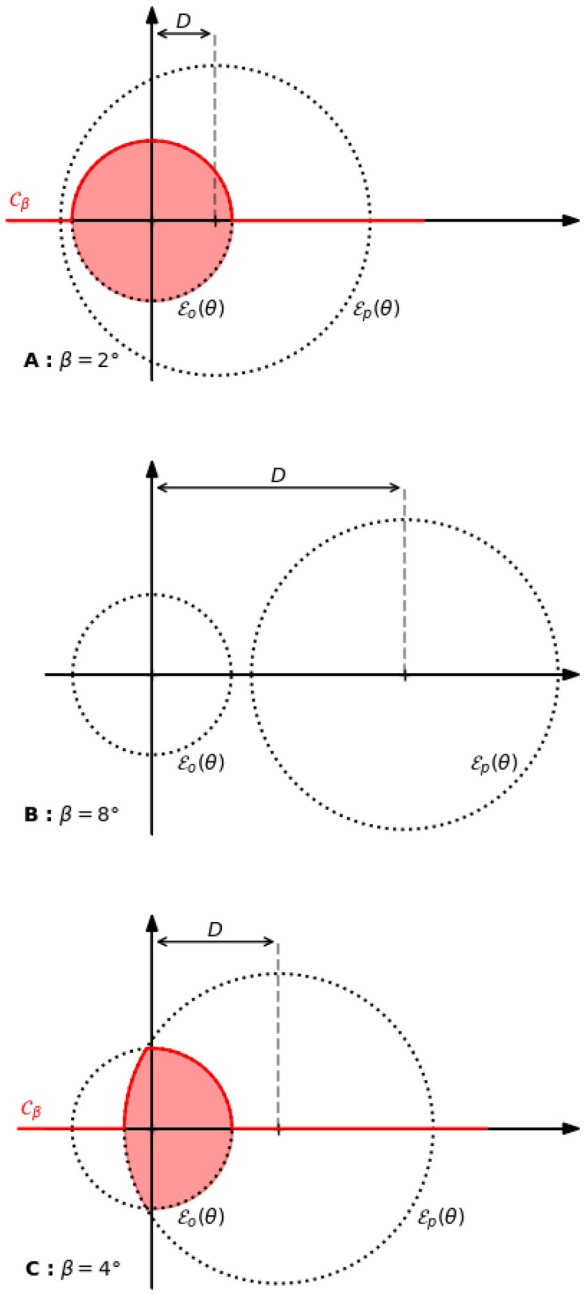

FIG. 5. Observation of the recovering area of the ellipses formed by the collector and the opening of the probe for angles illustrating the different cases to consider.

The equations of those two ellipses, $\mathcal{E}_o$ and $\mathcal{E}_p$, for the area of the opening and the plate, respectively, projected in the plane normal to the direction defined by the angle of approach β of an ion beam, are expressed as follows:

$$\mathcal{E}_o(\beta): \left\{ (x,y)\,|\, y = \sqrt{r_o^2 - \frac{x^2}{\cos(\beta)^2}} \right\},$$
$$\mathcal{E}_p(\beta): \left\{ (x,y)\,|\, y = \sqrt{r_p^2 - \frac{(x-D)^2}{\cos(\beta)^2}} \right\},$$

$\mathcal{E}_o(\beta)$ and $\mathcal{E}_p(\beta)$ are plotted in Fig. 5 for different values of β. For more readability, $\mathcal{C}_\beta(x)$ is introduced in this figure. This function represents the envelope of the intersection between $\mathcal{E}_o$ and $\mathcal{E}_p$. Hence, the overlapping area is

$$\mathcal{A}'(\beta) = \frac{2}{\pi r_o^2} \int_{-\infty}^{+\infty} \mathcal{C}_\beta(x)\mathrm{d}x. \tag{1}$$

Three cases are to be distinguished to compute Eq. (1).

In the first case, noted as A in Fig. 5, the opening ellipse is inside the collector one. This case stands for small angles β that satisfy the following relation:

$$D - r_p\cos(\beta) + r_o\cos(\beta) \le 0$$
$$\iff |\beta| \le \arctan\left(\frac{r_p - r_o}{\ell}\right).$$

The acceptance then takes the following value, $\mathcal{A}_{\mathcal{E}_o}$, as the area of the opening ellipse:

$$\mathcal{A}'(\beta) = \frac{\mathcal{A}_{\mathcal{E}_o}}{\pi r_o^2} = \frac{\pi r_o^2\cos(\beta)}{\pi r_o^2} = \cos(\beta).$$

In the second case, noted as B in Fig. 5, the two ellipses are disjointed and β satisfies the following relation:

$$D - r_p\cos(\beta) - r_o\cos(\beta) \ge 0$$
$$\iff |\beta| \ge \arctan\left(\frac{r_p + r_o}{\ell}\right).$$

In that case $\mathcal{A}' = 0$.

In the third case, noted as C in Fig. 5, when the ellipses partially overlap, the proper resolution of Eq. (1) is as follows:

$$\mathcal{A}'(\beta) = \frac{2}{\pi r_o^2} \int_{-\infty}^{+\infty} \mathcal{C}_\beta(x)\mathrm{d}x,$$
$$\iff \mathcal{A}'(\beta) = \frac{2}{\pi r_o^2} \int_a^b \min_x\big(f_o(x), f_p(x)\big)\mathrm{d}x,$$
$$\begin{cases} a = D - r_p\cos(\beta), \\ b = r_o\cos(\beta), \\ f_o(x) = \sqrt{r_o^2 - \dfrac{x^2}{\cos(\beta)^2}}, \\ f_p(x) = \sqrt{r_p^2 - \dfrac{(x-D)^2}{\cos(\beta)^2}}. \end{cases}$$

This integral is calculated numerically.

However, the opening ring has a non-negligible thickness, $\ell' = 1$ mm, as shown in Fig. 4. To find the opening area $\mathcal{O}$, a similar geometrical problem is to be solved, finding the intersection area between two ellipses of major axis r_o and minor axis $r_o\cos(\beta)$ separated by a distance $D = |\ell'\sin(\beta)|$. $\mathcal{O}$ is then multiplied with $\mathcal{A}'$ to get the true theoretical acceptance function $\mathcal{A}$ of the directional Faraday cup.

The theoretical value of $\mathcal{A}$ and of $\mathcal{O}$ is plotted in Fig. 6. To verify the exactitude of this description of the probe acceptance, both numerical computations using the software SIMION and measurements using an ion source are led. These results are presented in the two upcoming subsections.

2. The software SIMION in ideal regime

We use the software SIMION[24] to get a better understanding of the particle behavior inside and around the FCDi. This software simulates the trajectories of charged particles with a given energy distribution in a potential array defined by the user. A mesh of the FCDi is generated, respecting its physical dimensions. The potential of the plate, cylinder, and ring can be adjusted and the domain is surrounded by walls at potential 0 V far from the probe ($>10^3 r_o$). To perform meaningful simulations, we simulate the trajectory of a significant quantity of Xe^+ ions with a Gaussian initial energy distribution centered at 190 eV and with a standard deviation of 15 eV. Such a distribution is representative of the ion energy distribution measured using

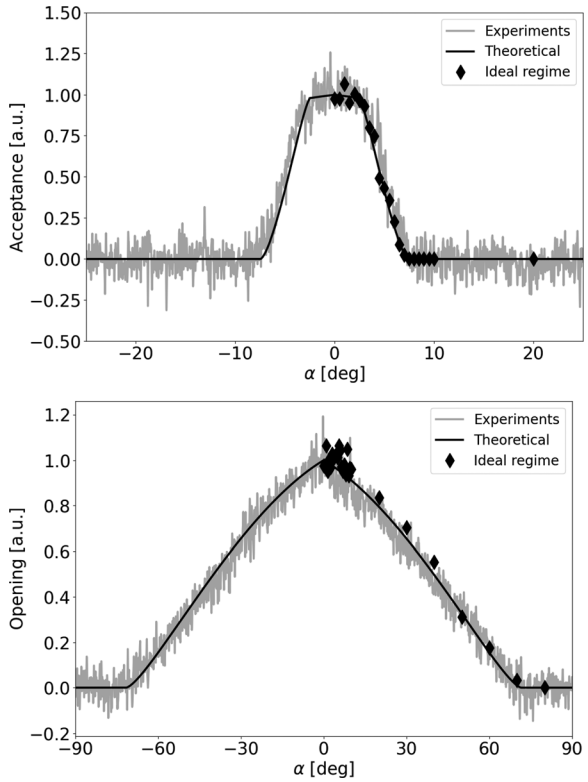

FIG. 6. Theoretical acceptance and opening functions of the FCDi (black solid lines) compared with ballistic simulation (scattered symbols) and experimental measurements during an α scan in front of a calibrated ion source (gray solid line).

an ion energy analyzer in the plume of the ECR thruster at 1 sccm of flow rate and 30 W of microwave power. The initial direction of the particles can be adjusted to make a certain angle with the probe entrance. When it hits a surface, a particle disappears and its position is recorded. The number of particles that hit the plate and the cylinder is then counted and divided by the number of particles that should theoretically have entered the probe at normal incidence. These two numbers define the simulated acceptance and opening. In the ideal regime, no bias is applied to the electrodes. Consequently, there are no potential arrays simulated and all ions have then a linear trajectory which is not modified by any effect.

3. Experimental approach with the ion source

The ion source introduced in Sec. II C is used to produce experimental material and confront the theory. A X_e^+ mono directional and mono energetic beam with an energy of 300 eV is generated. In front of the source, the FCDi is mounted on a stepper motor, and both the plate and the cylinder are biased at −100 V while the opening ring is grounded. The value of this bias voltage is chosen sufficiently low so that no remaining electrons can enter the probe, but not too low, so as not to affect the trajectory of the ions. The objective of this experiment is to be as close as possible to the ideal regime. The current drawn by the probe during its rotation in front of the ion beam is recorded.

4. Comparison of the different approaches in ideal regime

As the theoretical description of the acceptance and opening functions of the FCDi are purely geometric, the ideal regime is best suited to compare the theory with simulations. $\mathcal{A}(\alpha)$ and $\mathcal{O}(\alpha)$ derived in Sec. III B 1 are plotted in Fig. 6. On those figures, the scattered symbols are the simulation results obtained with the software SIMION. The gray lines, labeled Experiments, are the measurements of the current flowing, respectively, to the plate and the collector of the FCDi during a scan in front of the ion source (i.e., an α scan). The signals are normalized to allow a comparison with the theory.

A good agreement is observed between the model and the simulations. It confirms that the implementation of the dimensions and the mesh of the probe into the software as well as the number of simulated particles is sufficient to produce a meaningful behavior of the FCDi. Moreover, the comparable results obtained experimentally with the ion source prove that the FCDi is able to select the particles according to their trajectory in the presence of a mono energetic beam of ions. This feature is due to the narrow shape of the acceptance (half width at half maximum of 4.6°) and must remain valid in the plasma regime to assess the angular distribution of the plasma ejected in the magnetic nozzle of the ECR thruster. In fact, due to plasma effects, the shape of the acceptance in the plasma regime is *a priori* different from the theoretical value and may not be as narrow. This point is verified in Sec. III C. Guidelines concerning the probe utilization and bias voltages are given to ensure that the acceptance in the plasma regime is sufficiently narrow to enable the probe to select particle with their direction.

C. Probe collection in plasma regime

In the plasma regime, the electron population will interfere in the ion current collected by the probe in several ways. First, electrons can be collected by the probe, virtually reducing the measured ion flux. To prevent this, the probe collections have to be biased negatively. However, differences in the biasing applied to the probe collectors are the source of electric fields inside and outside the probe, modifying the trajectory of the ions impacting it, i.e., modifying the acceptance and opening functions. Second, the presence of electrons implies the formation of a plasma sheath in front of the probe and modifies the value of the ion flux and the ion trajectories. These two effects are studied experimentally and numerically, and the findings are detailed in the Secs. III C 1–III C 3.

In the remainder of the paper, an α scan (or angular scan) stands for the measurement of the ion current density in the plume of the ECR thruster during a rotation of the directional Faraday cup around its axis with the stepper motor. In the plasma regime, the ion current density is not *a priori* mono-directional and has an angular distribution noted as Φ. The asymptotic cases are an isotropic Φ, where the probe would measure an identical current for every α positions and a mono-directional Φ, where the acceptance and opening function would be retrieved along the alpha scan. Because the acceptance has a certain width, a one dimensional mathematical approximation of the quantity actually measured by the probe plate is the convolution between the acceptance of the probe and Φ. It reads as follows:

$$j_i(\alpha) = \int_{-\frac{\pi}{2}}^{\frac{\pi}{2}} \Phi(\beta)\mathcal{A}(\beta-\alpha)\mathrm{d}\beta \tag{2}$$

$$= [\Phi * \mathcal{A}](\alpha). \tag{3}$$

With such a formulation, it shows that a wider acceptance translates into a wider function $j_i(\alpha)$ measured by the FCDi during an angular scan.

1. Probe collector biasing

To determine at which voltage to bias the plate of the FCDi during an α scan, a current–voltage curve in cup mode (sum of the plate and cylinder current) is realized. The bias voltage of the plate and the cylinder is swept with the cup placed in front of the ECR thruster. Results are presented in Fig. 7 for several operating conditions of the thruster. The y-axis represents the current normalized by the ion saturation current, which is determined thanks to a linear fit of the ion

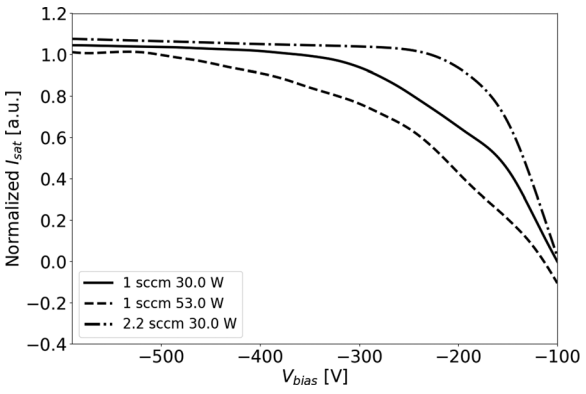

FIG. 7. Current normalized by the ion saturation current vs biasing voltage of the FCDi in cup mode facing the ECR thruster for different operation conditions.

saturation region (left part of the I-V curve). In this figure, it appears that under a normal thruster operating condition (1 sccm 30 W) as well as for high mass flow rate (2.2 sccm 30 W), a biasing voltage lower than −350 V is sufficient to collect only the ions and repel all of the electrons. However, at high power (1 sccm 53 W), a biasing voltage lower than −500 V must be applied to the FCDi. It is due to the high-energy tail of the electrons' energy distribution function. In the remainder of this paper, the bias voltage of the plate of the FCDi is set to $V_b = -350$ V for all the thruster operating conditions except for the data point made at 1 sccm 53 W, where it is set to $V_b = -500$ V. The influence of the cylinder and the ring bias voltages different from V_b on the current collected by the plate is assessed in Sec. III C 2. Considering that the ion energy in the plume of the ECR thruster is typically between 100 and 200 eV, particle deflections inside and around the FCDi are to be expected when its collectors are biased at low voltage. Therefore, it is reasonable to think that the true acceptance and opening functions of the probe vary when changing the bias voltages of its different parts. Two effects should be considered. On the one hand, deflections that happen inside the probe modify the acceptance and opening functions but leave the current collected in cup mode unaffected. On the other hand, particles are also likely to be deflected in front of the probe due to the formation of a plasma sheath whose depth is not negligible compared to the probe dimension. These questions will be assessed in the next two subsections by means of numerical simulations and experimental measurements.

2. Numerical simulation of the plasma regime with the software SIMION

The software SIMION is not intended to simulate the plasma–wall interactions and even if electrons are introduced and sent to the probe, no plasma sheath is computed by the software. The electric fields present in the simulation domain are computed based on the initial potentials of the collectors in vacuum. Therefore, to reproduce the effect of a sheath that forms in front of the probe, a grid fully transparent to particles with a potential fixed at 0 V is placed in front of the probe to ensure that the potential fall occurs within a few probe opening radii. Given the plasma parameters in the plume of the ECR thruster, it corresponds to several Debye lengths. The distance between the grid and the probe can be adjusted to simulate different sheath thicknesses.

Four simulation cases illustrate the behavior of the FCDi immersed in a plasma for different parameters of operation to be tested and are reported in Fig. 8. The bias voltages of the plate V_{plate}, the cylinder V_{cyl}, and the ring V_{ring} are changed between the different simulations and the amount of current extracted by the different collectors are analyzed.

(i) The plate and cylinder are biased at different voltages, −300 and −100 V, respectively, and the ring is left at 0 V. An electrostatic lens is present at the bottom of the probe [Fig. 8(b)], bending the particle trajectories and increasing the current drawn on the plate. This configuration is then discarded and the condition $V_{plate} = V_{cyl}$ is verified in the remainder of the paper.

(ii) The plate and the cylinder are both biased at −300 V as well as the ring. Two cases are simulated, without and with the grounded grid. Without the grid, a large electrostatic lens develops in front of the probe that increases the amount of ions entering the probe by focusing the beam [Fig. 8(c)]. The particle deviation in front of the probe induces an artificial increase in the opening function and the level of current collected by the collectors. With the grid, the electrostatic lens

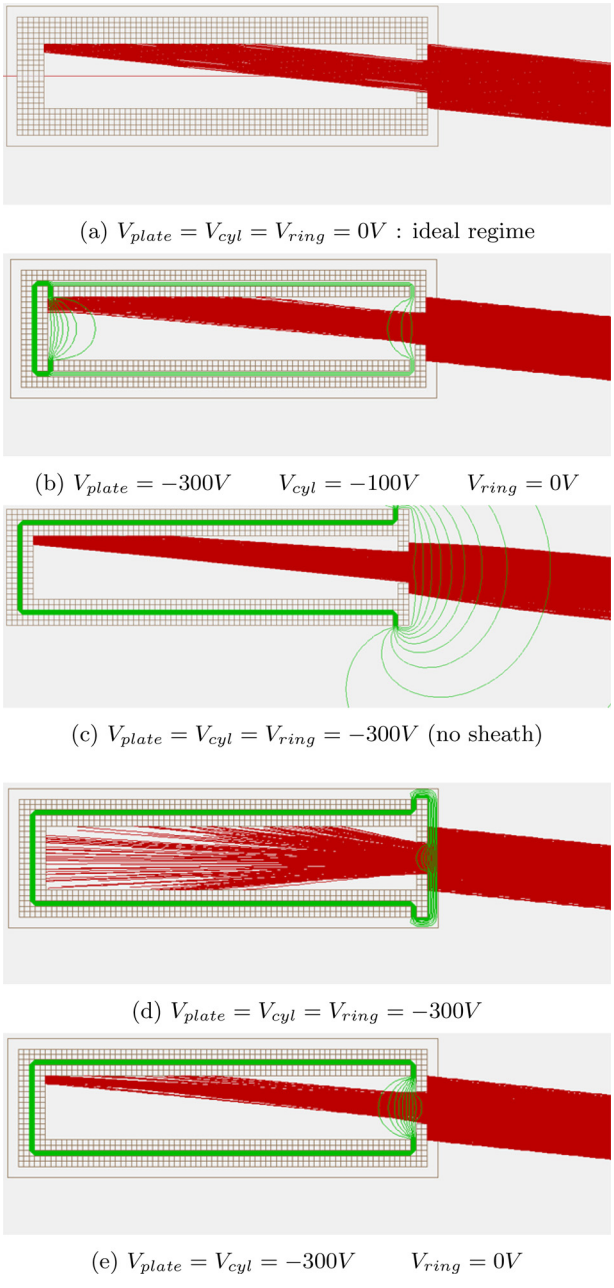

FIG. 8. Simulation cases illustrating the behavior of ions entering the FCDi for several biasing conditions. The red lines represent the ion trajectories. Iso-potentials are represented in green (a) $V_{plate} = V_{cyl} = V_{ring} = 0$ V: ideal regime, (b) $V_{plate} = -300$ V, $V_{cyl} = -100$ V, and $V_{ring} = 0$ V, (c) $V_{plate} = V_{cyl} = V_{ring} = -300$ V (no sheath), (d) $V_{plate} = V_{cyl} = V_{ring} = -300$ V, and (e) $V_{plate} = V_{cyl} = -300$ V $V_{ring} = 0$V.

outside of the probe is suppressed but another one appears at the probe entrance that diffracts the ion beam inside the probe [Fig. 8(d)]. Even though this effect does not change the current collected in the cup mode, it strongly affects the acceptance function and induces a loss of angular selectivity of the probe in directional mode.

(iii) The plate and the cylinder are biased at the same voltage (−300 V), the ring is grounded (0 V), and the simulation is performed with the grid. In this case, the electrostatic lens effect is limited due to the ratio between the entrance size of the probe and the diameter of the lens [Fig. 8(e)]. This configuration seems to be the best way to measure a meaningful ion current in cup mode while keeping the angular selectivity of the probe in directional mode.

To allow the confrontation of cases simulated in Figs. 8(d) and 8(e) to experiments, complete acceptance functions are simulated with SIMION for four different opening ring voltages bias and with the plate and cylinder biased at −300 V. A transparent grid kept at 0 V is placed in front of the probe entrance at a distance equal to the opening radius [same configuration of Fig. 8(e)]. Results are presented in Fig. 9. As expected, the more negatively biased the opening ring, the wider and lower the acceptance. This phenomenon is due to the burst of the beam inside the probe that is more pronounced when the ring bias voltage becomes more negative.

3. Experimental approach with the ECR thruster

To verify the simulation outcomes, α scans are performed in front of the ECR thruster at $\theta = 0$. The opening ring is biased at various negative voltages as done in the simulations. Results presented in Fig. 10 are angular scans realized in the thruster plasma, they represent the local ion current density expressed by $j_i(\alpha)$ measured by the FCDi. Only a qualitative agreement with the numerical simulations, consisting in similar evolution of profiles, could be expected. The ion current density is also measured with a guard ring Faraday probe (FPGR) at the same location with normal incidence of the ECR thruster ($\alpha = 0$, $\theta = 0$).

As observed in the simulations, when the biasing of the opening ring is getting more negative and closer to the plate and cylinder biasing, the measured plate current scan is decreasing in the center of the scan ($\alpha = 0$) and widening on its sides. This result is in line with the burst of the ion beam observed in Fig. 8(d) and with a wider acceptance function. These measurements do not ensure that the acceptance function has remained unperturbed while going from the ideal case to the plasma case but allow to select the operation regime of the probe that limits an eventual perturbation. In addition, the cup current, i.e., sum of the plate and cylinder currents, remains constant at the scan center ($\alpha = 0$). It confirms the fact that particle deflections induced by the biasing of the opening ring mainly occur inside the probe. On the contrary, the cup current increases at high α angles (about 30° and above) as the ring biasing decreases. This is believed to be due to ion deflection toward the probe at high approaching angles. Finally, the current collected by the FPGR biased at −350 V and placed in front of the thruster exit is larger than the FCDi current in cup mode at $\alpha = 0$. This point will be examined in more detail in Sec. V.

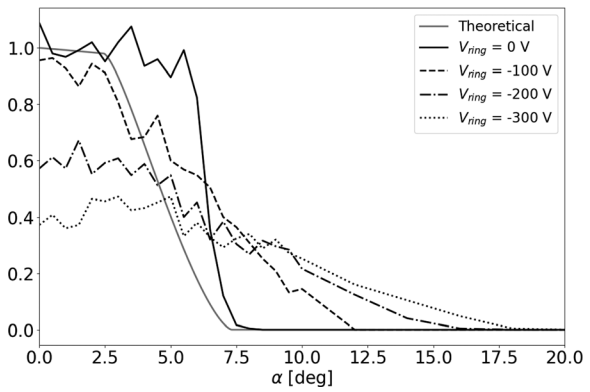

FIG. 9. Acceptance of the FCDi simulated with SIMION for several values of V_{ring}.

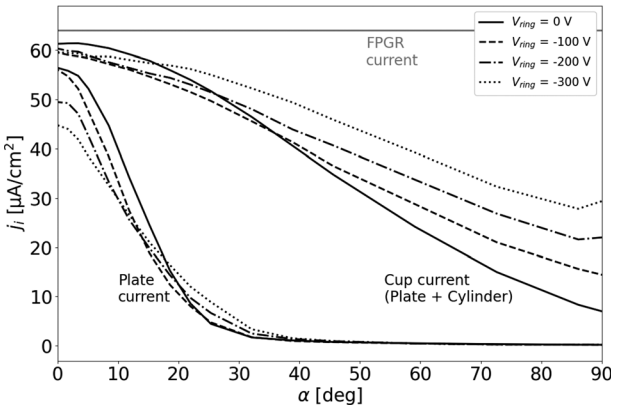

FIG. 10. α scans performed with the directional Faraday probe at $\theta = 0$ for several values of V_{ring}.

Results presented in Sec. III suggest that the FCDi can be used to characterize the local ion current density produced by the ECR thruster. The probe plate and cylinder must be biased at the same voltage and sufficiently negatively to ensure ion saturation current collection, namely, −350 V (−500 V at high thruster power). The ring must be kept close to 0 V and will be tight to ground in the remainder of this paper to minimize perturbation of the acceptance function of the probe. These developments will be used in Sec. IV to investigate the accuracy of the indirect estimation of the thrust produced by the ECR thruster by comparing it to direct thrust measurements.

IV. DIRECT AND INDIRECT THRUST MEASUREMENTS OF THE ECR THRUSTER

A. Direct thrust measurement methodology

The thrust stand used in this study to measure the thrust of the ECR thruster is a simple pendulum balance where eight thin beryllium copper strips ensure a single degree of freedom. It is represented in Fig. 11. The arm of the balance, where the ECR thruster is mounted, is 332 mm long and kept in position thanks to a magnet and a coil whose voltage is regulated by a Proportional–Integral–Derivative (PID) system. When the thruster generates a horizontal force, the voltage needed to keep the arm steady increases. Therefore, a PID voltage drop is observed when the thruster is shut off.

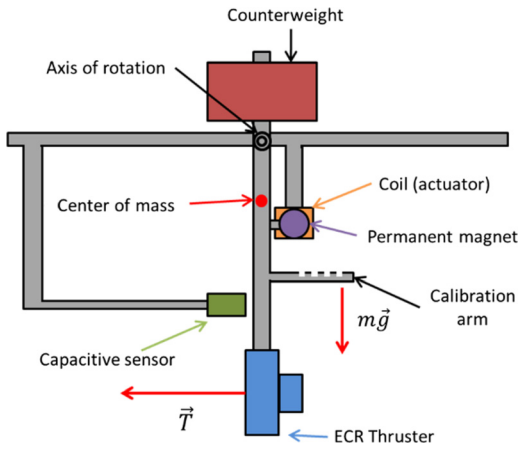

FIG. 11. The thrust stand in the B09 facility. Reproduced with permission from Vialis *et al.*, J. Propul. Power **34**, 1323–1333 (2018). Copyright 2018 American Institute of Aeronautics and Astronautics, Inc.

The PID voltage drop V_{PID} is related to the thrust T of the thruster by the linear relation $T = \gamma V_{\mathrm{PID}}$, where γ is a calibration factor obtained thanks to the deposition and the retrieval of five well known weights on the arm of the balance at precise locations. As the mass and position of each weight are known, the force imparted on the arm after the deposition and retrieval of the weights is linked to a drop of V_{PID} to get γ. This calibration phase takes place before each batch of thrust measurements. More details on the thrust balance setup and operation can be found in Ref. 19. This balance has been proven reliable in several studies, therefore, it is considered to give a reference of the thrust of the ECR thruster throughout the remainder of the paper. The relative error on direct thrust measurements is below 5%. It is due to the thermal equilibrium of the system, the mass and the position of the weights during the calibration phase.

B. Indirect thrust measurements methodology

The thrust of the ECR thruster can be evaluated from ion current density and velocity measurements. Indeed, it is due to the ejection of the plasma from the source at high velocity. A reasonable assumption is to consider that the contribution of electrons to the thrust is negligible regarding their weak mass compared to the ions. The neutrals' contribution to the thrust can also be neglected because they are not accelerated in the magnetic nozzle and have, therefore, a small velocity compared to the ions. The elementary thrust δT_z is written as the force of the plasma pressure produced on a small surface δS located downstream of the thruster ejection.[20] It reads as follows:

$$\begin{aligned}\delta T_z &= \delta T\cos(\theta) = P_{\mathrm{plasma}}\delta S\cos(\theta)\\ &= m_i n_i v_i^2\cos(\theta)\delta S,\end{aligned} \tag{4}$$

where m_i, n_i, and v_i are the ion mass, density, and velocity, respectively. It is supposed here that the presence of multiple charged ions is negligible. Moreover, v_i is taken to be the most probable ion velocity from ion energy analyzer measurements. The thrust T is obtained by integrating δT_z over half a sphere of radius ρ noted as $\mathcal{S}_\rho$. Considering the cylindrical geometry of the plasma source, we suppose that the ejection region is axisymmetrical so T is retrieved from only one angular scan of the ion current density along θ as follows:

$$\begin{aligned}T &= \int_{\mathcal{S}_\rho}\delta T_z,\\ &= \int_{\phi=0}^{\phi=\pi}\int_{\theta=-\frac{\pi}{2}}^{\theta=\frac{\pi}{2}}\delta T_z\rho^2\cos(\phi)|\sin(\theta)|\mathrm{d}\phi\mathrm{d}\theta\\ &= \pi\rho^2\int_{-\frac{\pi}{2}}^{\frac{\pi}{2}} m_i n_i v_i^2\cos(\theta)|\sin(\theta)|\mathrm{d}\theta\\ &= \pi\rho^2\frac{m_i v_i}{e}\int_{-\frac{\pi}{2}}^{\frac{\pi}{2}} j_i(\theta)\cos(\theta)|\sin(\theta)|\mathrm{d}\theta.\end{aligned} \tag{5}$$

Here, $j_i = e n_i v_i$ is the ion current density and the axisymmetry hypothesis is made. The ion velocity is supposed not to depend on the angle θ, this hypothesis has been proven valid for $\theta \in [-45; 45]$ with retarding field energy analyser[21] and more recently with LIF measurements.

Equation (4) implies that ions are ejected from the thruster with a radial trajectory. This assumption may be satisfactory for EP technologies such as GIT and HET, where the acceleration of ions occurs in a small region close or inside the discharge region. After they exit the thruster, the ions then propagate following a straight trajectory almost purely radial from an ejection point located at the center of the thruster in its exit plane. Equation (4) also neglects the effect of charge exchange collisions. However, in the case of the ECR thruster, and this may be generalized to magnetic nozzle (MN) thrusters, ions may not be ejected radially from the thruster source. In fact, the plasma may stay magnetized along a certain distance from the thruster in the MN and charges may follow a bent trajectory according to the geometry of magnetic field lines.

Figure 12 shows α scans measured with the plate of the FCDi at positions $\theta = -15°$, $\theta = 0°$, and $\theta = 12.5°$ in the plume of the ECR thruster operating at 1 sccm of xenon mass flow rate and 20 W of power. To determine the most probable ion flux direction at a given position θ, an algorithm finds the middle between the ascending and descending slopes of the α scan. It is more precise than the position of the maximum of current because α scans are not *a priori* symmetrical. The function $\alpha_{\mathrm{mean}}(\theta)$, thus determined, is plotted in Fig. 13. It shows that the hypothesis of radial ejection of the ions is not valid. Indeed,

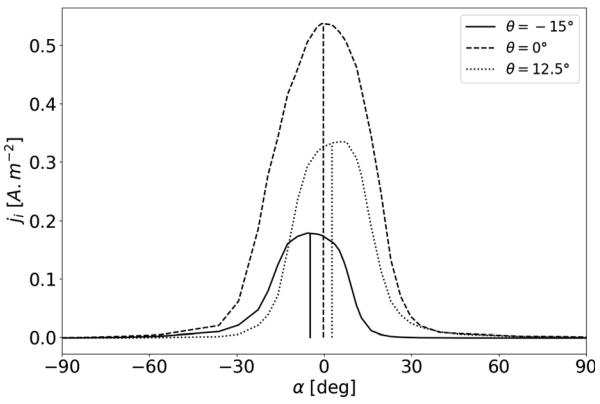

FIG. 12. Example of three α scans made at different angular positions of θ and the most probable ion direction associated.

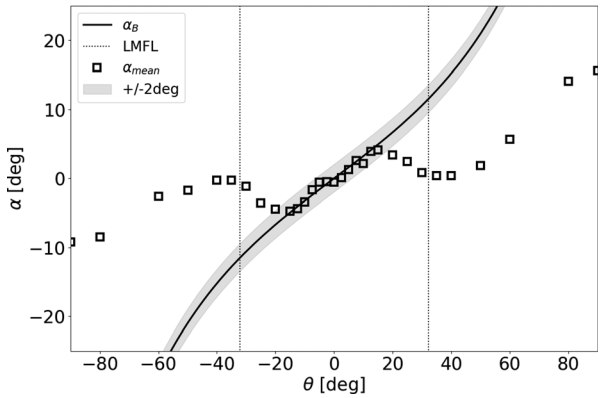

FIG. 13. Most probable direction of ions determined for each α scan made at different angular positions of θ.

α_{mean} would be 0 for every position θ in this case. Instead, α_{mean} varies from -10 to $+10°$ along the θ scan for this experimental condition. This observation is further discussed in Sec. V F.

To take into account the fact that ions do not follow the radial direction, three different variations of the integral term of Eq. (5) are introduced to compute the indirect thrust of the ECR thruster with several degrees of complexity. They account for the direction of the probe when the measurement is done and the projection along the most probable direction of the ion flux; the variations are expressed as

$$T_A \propto \int_{-\frac{\pi}{2}}^{\frac{\pi}{2}} j_i(\theta, 0)\cos(\theta)|\sin(\theta)|\mathrm{d}\theta, \tag{6}$$

$$T_B \propto \int_{-\frac{\pi}{2}}^{\frac{\pi}{2}} j_i(\theta, \alpha_{\text{mean}}(\theta))\cos(\theta)|\sin(\theta)|\mathrm{d}\theta, \tag{7}$$

$$T_C \propto \int_{-\frac{\pi}{2}}^{\frac{\pi}{2}} j_i(\theta, \alpha_{\text{mean}}(\theta))\cos(\theta + \alpha_{\text{mean}}(\theta))|\sin(\theta)|\mathrm{d}\theta. \tag{8}$$

In Eq. (6), the Faraday probe current is taken at $\alpha = 0$ for each position θ and the projection is radial. With the same projection, the Faraday probe current is taken at $\alpha = \alpha_{\text{mean}}$ in Eq. (7). Eventually, the expression that most precisely takes into account the ion trajectories is Eq. (8), where the Faraday probe current is taken at $\alpha = \alpha_{\text{mean}}$ and projected along the ion direction $\theta + \alpha_{\text{mean}}$.

C. Comparison between direct and indirect thrust measurements

A reliable indirect thrust measurement method should output results comparable with direct thrust measurements over the whole range of xenon mass flow rate and microwave power accessible to the operation of the thruster. These two operation parameters are then varied on large intervals of accessible values, from 20 to 48 watts for the microwave power and from 0.6 to 2.4 sccm for the flow rate. The version of ECR thruster used in this study has been shown to be most efficient at 1 sccm of xenon mass flow rate and 30 W of power.

The relative errors between direct and indirect thrust measurements for a range of microwave power at a constant mass flow rate of 1 sccm and a range of mass flow rate at a constant power of 30 W are displayed on Figs. 14(a) and 14(b), respectively. Data points labeled

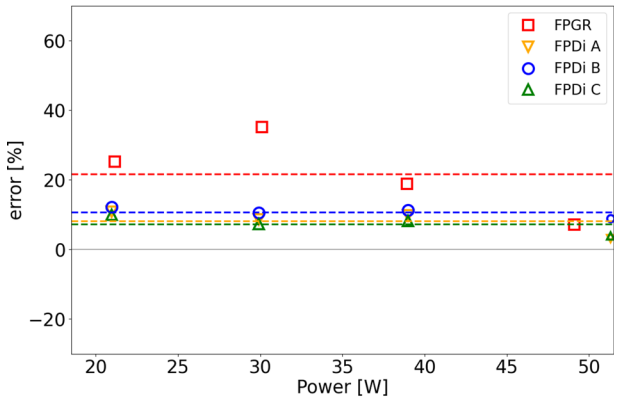

(a) Constant mass flow rate of 1 sccm.

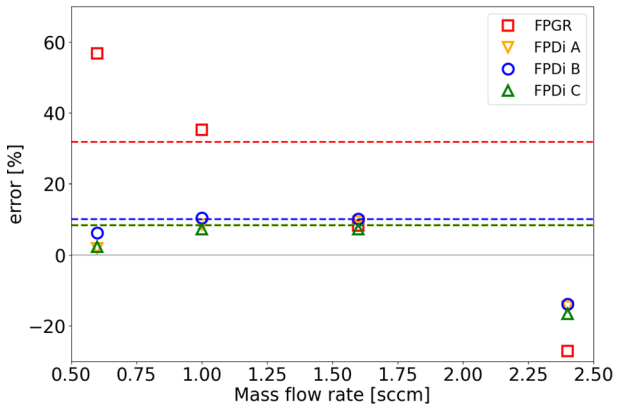

(b) Constant power of 30 W

FIG. 14. Relative errors between direct and indirect thrust measurements. Dashed lines indicate the mean of the absolute value of the data points for each cases. (a) Constant mass flow rate of 1 sccm. (b) Constant power of 30 W.

FCDi A, B, and C correspond to the current density being measured using the FCDi and thrust computed expressions T_A, T_B, and T_C of Eqs. (6)–(8), respectively. Data points labeled FPGR correspond to Eq. (5) where the ion current density has been measured with the Faraday probe with guard ring.

To compare those four cases of study between each other, the mean of the relative errors in absolute value is represented with dashed lines. The values are also recalled in Table I to ease the analysis.

The three levels of complexity (A, B, and C) for the computation of the thrust from directional Faraday cup data lead to an average value of the absolute errors of the same order and close to 10%. These measurements largely improve the level of error obtained with the

TABLE I. Relative errors (in %) made on the thrust for different indirect thrust measurement methods.

	FPGR	FCDi A	FCDi B	FCDi C
Constant mass flow rate	21.70	8.10	10.68	7.24
Constant power	31.84	8.65	10.14	8.35

measurements obtained with the Faraday probe with guard ring that is about 20% and 30% for the two datasets. It is also observed that the errors for the FPGR measurements present trends with thruster power and mass flow rate that are largely damped by the usage of the FCDi. Outlying points up to 35% and 60% for the FPGR datasets are reduced to 10% for the measurements with the FCDi.

Comparing more closely the errors computed from the three ways of estimating the indirect thrust (A, B, and C), very similar averaged errors are obtained with expressions T_A and T_B, and a small decrease in the average error is observed for T_C (Table I).

V. DISCUSSION

A. Improvement of indirect thrust measurement accuracy

This work demonstrated, by the development and testing of a new type of Faraday cup, that the ion flux ejected from an ECR thruster is not radially emitted. The modification of the indirect thrust measurement expression to take into account this phenomenon and the comparison with direct thrust measurement shows that this characteristic does not contribute significantly to indirect thrust measurements errors. In fact, taking into account the ion flux in the most probable direction of ejection α_{mean} at each θ does not improve significantly the measurement accuracy [comparison between T_A and T_B in Figs. 14(a) and 14(b) and Table I]. Similarly, taking into account the local most probable angle of the ion flux seems to improve very marginally (about 1.5%) the accuracy of the indirect thrust measurements [comparison between T_B and T_C in Figs. 14(a) and 14(b) and Table I]. As Fig. 13 shows, $\alpha_{\text{mean}}(\theta)$ is always the same sign as θ, meaning that $\cos(\theta + \alpha_{\text{mean}}(\theta)) < \cos(\theta)$. Thus, taking into account the ion flux, local direction has the effect of decreasing marginally the indirectly estimated thrust. These two conclusions invalidate the initial hypothesis supporting that the non-radial ejection of ions in the ECR plume might be the cause of the overestimation of the thrust by indirect measurements using FPGR.

Comparing the indirect thrust obtained from FPGR and FCDi measurements demonstrates a drastic improvement in the accuracy of the indirect thrust measurements with an overall reduction of the estimated thrust. The dataset obtained with the FPGR and the dataset presenting T_A indicate that FPGR measurements are likely to overestimate the ion current in the plume of the ECR thruster. These results allow to define a recommendation to measure the thrust of an ECR thruster by means of probes which is to use a Faraday cup instead of a planar Faraday probe. Such usage reduces the uncertainties below 10%, which represents a great improvement with respect to a previous situation. The possible reason for such an improvement of the accuracy is analyzed in Sec. V B.

B. Origin of the discrepancy resulting from Faraday probe with guard ring measurements

Results presented in Figs. 14(b) and 14(a) and Eq. (5) suggest that the differences observed in the comparison between direct and indirect thrust measurements is due to an overestimation of the current density by the FPGR. Figure 15 compares the integrand of Eq. (5) for the FPGR and FCDi measurements in the plume of the thruster firing at 20 W and 1 sccm. The results are normalized to 1 at the maximum to show the different shapes of the signal measured with the FCDi and

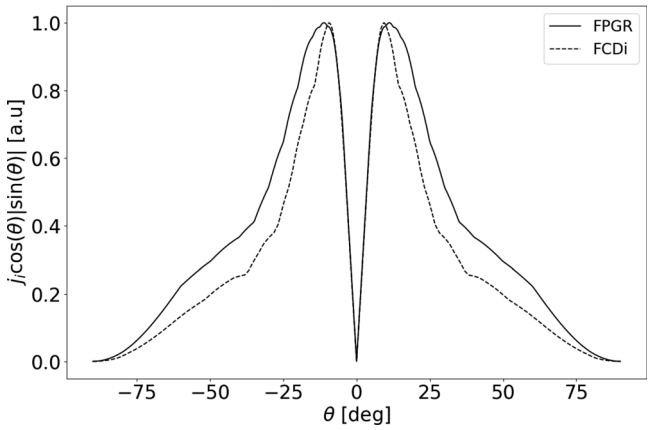

FIG. 15. Comparison between the integrand of Eq. (5) where j_i is the current measured with the Faraday probe with guard ring (FPGR) and the directional Faraday probe (FCDi) at 20 W and 1 sccm.

the FPGR. The overestimation of current induced by the FPGR mainly occurs at large values of θ in the plume of the ECR thruster.

The FPGR was designed according to the recommended practice of Ref. 8 that advises to take a guard ring diameter $\varnothing_{\text{FPGR}}$ superior to 50 times the Debye length λ_D of the plasma. However, in the conditions of biasing potential of the FPGR presented here, the size of the sheath forming in front of the probe may be governed by the Child–Langmuir sheath law. The thickness of the sheath s_{CL} that forms in front of a wall at potential V_0 is as follows:

$$s_{CL} = \frac{2}{3}\sqrt{\frac{\epsilon_0}{j_i}}\left(\frac{2e}{m_i}\right)^{1/4} V_0^{3/4}. \tag{9}$$

It defines another criterion that should be satisfied which is that the Child–Langmuir sheath thickness must be low compared to the guard ring radius, i.e., $\varnothing_{\text{FPGR}}/s_{CL} \gg 1$. If not, border effects induce a non-flat sheath that is likely to bend the trajectories of the ions approaching the surface of the probe and induce an artificial increase in the current collected.

To investigate the effect of a sheath in front of the FPGR, simulations are carried out with the software SIMION as presented in Sec. III. The acceptance of the FPGR is simulated for several $\varnothing_{\text{FPGR}}$ to s_{sheath} ratios, where s_{sheath} is the position of a transparent grid biased at 0 V placed all around the probe. The results are presented in Fig. 16 along with the simulation in an ideal regime (no bias applied) and the theoretical acceptance of the FPGR, which is a cosine in the range $-\pi/2 \leq \beta \leq \pi/2$ and 0 elsewhere.

Figure 16 shows that the ratio $\varnothing_{\text{FPGR}}/s_{\text{sheath}}$ should be at least six to neglect effect of the sheath thickness on the acceptance function of the FPGR. This value is only an order of magnitude, a quantitative analysis of the error induced by the presence of a sheath in front of the FPGR would require more precise simulations involving a thorough plasma behavior description. This would be achieved with particle in cell (PIC) simulations for example.

The comparison between the Debye length and the Child–Langmuir sheath thickness with the diameter of the probe is shown in Fig. 17 along with the θ scan of the experimental conditions of 20 W of power and 1 sccm of mass flow rate. Two hypothesis are made to

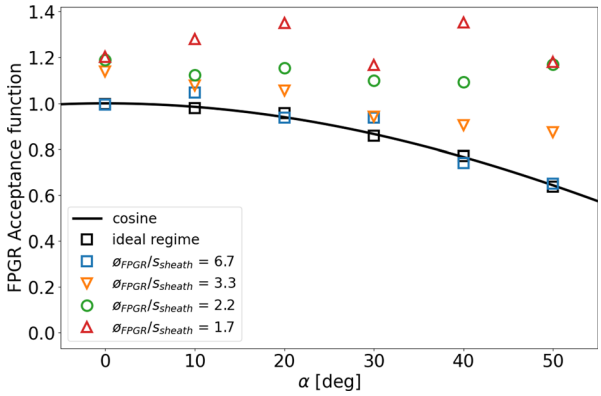

FIG. 16. Theoretical acceptance function (black solid line) of the FPGR with acceptance simulated with SIMION in ideal regime (black squares) and in the presence of a grounded grid for several $\varnothing_{FPGR}/s_{sheath}$ ratios.

compute λ_D. One the one hand, the ion energy is not supposed to depend on the angle θ, therefore, the ion velocity is $v_i = \sqrt{2eE_i/m_i}$. On the other hand, the ion and electron densities are supposed to be equal. Hence, because $j_i = en_iv_i$, the Debye length is as follows:

$$\lambda_D = \sqrt{\frac{\epsilon_0 T_e}{en_e}} = \sqrt{\frac{\epsilon_0 T_e v_i}{j_i}}. \tag{10}$$

Figure 17 shows that the criterion $\varnothing_{FPGR}/50\lambda_D > 1$ is satisfied only for low electron temperatures and at the center of the plume of the ECR thruster, where the plasma density is higher. Moreover, the criterion $\varnothing_{FPGR}/s_{CL} \gg 1$ is not verified for the whole range of ion current density when the bias voltage of the probe is very low. Moreover, the dependence on $1/\sqrt{j_i}$ of both the Debye length and the Child–Langmuir thickness implies that the FPGR is likely to overestimate the ion current density where the ion density is low, i.e., far from the center of the plume for high values of θ. This is in line with the results presented in Fig. 15 and discussed above.

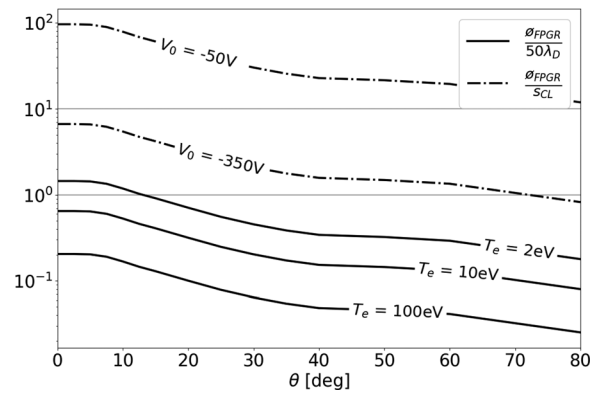

FIG. 17. FPGR guard ring diameter to fifty Debye length ratio (Brown criterion[8]) and Child–Langmuir sheath thickness to FPGR guard ring diameter ratio for several electron temperatures and probe bias voltages.

C. Secondary electron emission

The secondary electron emission (SEE) is often cited as a term to be corrected in electrostatic probe measurements. In fact, if electrons emitted are not recollected by the Faraday probe, which is likely with a planar FPGR biased at −350 V, the current measured by the probe is artificially increased. The SEE yield coefficient for Xe^+ and Xe^{2+} ions on molybdenum is around 0.02 and 0.2, respectively, for energies below 1 keV.[25] It induces an error of 2%–10% depending on the ratio of doubly ionized ions. Moreover, the cylinder of the FCDi is made of graphite, with an SEE yield coefficient lower than the molybdenum.[26] With the cup design, SEE is more likely to be recollected by the probe, which lowers the influence on the signal measured in cup mode. The influence of SEE cannot entirely explain the overestimation of the ion current density by the FPGR; however, it may be a contribution to the thrust estimation reduction obtained with the FCDi.

D. Presence of multiple charged ions

To assess the influence of the presence of multiple charged ions to the indirect thrust, the plasma can be considered to be constituted of singly charged ions of density n_I, velocity v_I, and energy E_I and doubly charged ions of density n_{II}, velocity v_{II}, and energy E_{II}. The parameter η is defined as the ratio between the densities of the two populations such that $n_{II} = \eta n_I$. Due to the assumptions made in Sec. IV B, the ratio between the indirect thrust estimated from ion current density measurements and the direct thrust is $K_{\text{multi}} = \frac{1+2\sqrt{2\eta}}{1+2\eta}$.

Measurements performed with an ion analyzer indicate that η is comprised between 0 and 0.1 in the range of thruster operating conditions tested. It leads to values of K_{multi} between 1 and 1.069, with an average of 1.03 that could explain the general overestimation of the indirect thrust observed in Fig. 14. These measurements also reveal that the presence of ions charged three times or more is negligible in the plume of the ECR thruster. The details of the calculation of K_{multi} are presented in the Appendix.

E. Evolution at high mass flow rates

It appears in Fig. 14(b) that at a high mass flow rate (2.4 sccm) the indirect thrust measurements computed using either the FPGR and the FCDi are lower than the direct thrust measurements, whereas they are generally higher in the other cases. A possible explanation of this observation is the rise of the vacuum chamber pressure and the diminution of the ion energy when the mass flow rate increases. These two factors increase both the neutral density encountered by the ion flux and the charge exchange cross section.[27] The mean free path of Xe^+ is then reduced and the ions are more likely to encounter a charge exchange collision during their acceleration in the magnetic nozzle of the thruster. Therefore, the plume of the thruster may contain a significant amount of neutrals at a high velocity that could contribute to the thrust without being measured by any ion collection probe.

The correction factor to apply to the thrust estimated with the indirect method due to the charge exchange collisions is $K_{\text{cex}} = \frac{1+\tau\sqrt{\kappa}}{1+\tau}$, where τ and κ are the ratio of the densities and energies, respectively, between the slow ions resulting from a charge exchange collision and the fast ions.

The factor K_{cex} is estimated for a range of thruster mass flow rates at a microwave power of 30 W. For mass flow rates lower than 1.6 sccm, K_{cex} is comprised between 0.91 and 0.97. However, for high

mass flow rates greater than 2 sccm, K_{cex} drops down to 0.75. Hence, the presence of neutrals at high velocity due to charge exchange collisions could explain the underestimation of the thrust calculated by the indirect method of more than 20% and the tendency observed in Fig. 14(b). This discrepancy between indirect and direct thrust measurements observed on both probes may then be due to the test conditions and not to the probe performances.

The notations and details of the calculation of K_{cex} are presented in the Appendix.

F. Ion trajectories in the magnetic nozzle

In Fig. 13, representing the function $\alpha_{mean}(\theta)$ for the 1 sccm, 20 W of power operation of the thruster, the angle $\alpha_B(\theta)$ is also represented. This angle is defined as the local angle a magnetic streamline makes with the radial direction at a given angular position θ on the arc of radius ρ. Moreover, the dashed lines labeled LMFL corresponds to the angle θ at which the last magnetic field line crosses this arc. The last magnetic field line is defined as the most diverging magnetic field line that does not intersect physically the source of the thruster (see Figs. 1 and 2 for the notations).

This figure reveals that there is no range of angles θ for which the value of α_{mean} is null. It demonstrates that the ions are not ejected radially from the thruster. Instead, for absolute values of θ smaller than 17°, corresponding to the center of the plasma plume, the ion flux direction is aligned with magnetic field lines. The ion trajectories are then strongly coupled to the MN topology, even 30 cm away from the thruster exit plane. At the edges of the plume, for θ angles larger than 17°, the angle between the ion flux direction and the radial direction is different and smaller than the angle between the magnetic field and the radial direction. It demonstrates that the ion trajectories are not governed by the MN topology in this region and that the plasma have undergone a demagnetization at smaller distance from the thruster. The fact that for positive values of θ, we have $\alpha_{mean} < \alpha_B$ (and conversely for negative values of θ) indicates that this detachment is converging. This preliminary result is in line with an inward detachment observed in the magnetic nozzle of the VASIMR thruster with a different approach[3] and is predicted by some numerical and theoretical work.[28–30] A more thorough analysis of this phenomenon is beyond the scope of this paper and will be the object of future investigations.

VI. CONCLUSION

A new type of electrostatic probe, the directional Faraday cup (FCDi) is introduced to study the plume of the ECR thruster developed at ONERA. This diagnostic benefits from an innovative design that allows to assess the angular distribution of ion current density in the plume of electric propulsion devices.

In the first part of this paper, a theoretical study of the FCDi is proposed. It is supported by both simulations and experiments and confirms the ability of the probe to select the ions collected according to their direction. Guidelines are given to choose the bias voltages that must be applied to the different parts of the probe in order to ensure the measurement of a meaningful ion current density. The opening ring must be grounded, while the plate and the cylinder must be biased at the same voltage with a value sufficiently low to ensure the collection of only ions. In the plume of the ECR thruster, for high power to mass flow rate ratio, the value of the bias voltage can be as low as −500 V.

The second part of the paper presents the first application of the FCDi. Direct and indirect thrust measurements are compared, with ion current measured with a planar Faraday probe with guard ring (FPGR) and with the FCDi. The overestimation of the thrust by the FPGR is confirmed with thrusts 20%–30% higher than direct thrust measurements. The usage of the FCDi allows to reduce this overestimation to 8%–10%. Results indicate that taking into account the local trajectories of the ions in the computation of the thrust gives a more accurate estimation by only 1%–2%, which suggests that the discrepancy originates from an overestimation of the current measured by the FPGR. The investigation indicates that this behavior comes from the large plasma sheath in front of the probe when biased at very low voltages. Secondary electron emission (SEE) does not appear to be a major effect in the indirect overestimation of the thrust by the Faraday probes since they are made of low SEE yield materials.

The presented data, acquired using the FCDi, also contributes to demonstrate that the ion flux ejected from the thruster is strongly affected by the magnetic nozzle. At 30 cm from the thruster, in the central part of the plume (for $\theta < 17°$), the ion flux direction is still co-linear to the magnetic field. For angles larger than 17°, the ion flux is not co-linear to the magnetic field but does not exhibit a trajectory typical of a radial ejection from the thruster source. It suggests that the ions may have been magnetized for smaller distances to the thruster but are demagnetized at 30 cm. Further analysis with measurements performed at different distances and with different thruster operating conditions could contribute to a better description of this phenomenon.

ACKNOWLEDGMENTS

The authors would like to acknowledge Simon Peterschmitt for the first design and the conception of the directional Faraday cup. They would like to thank Federico Boni and Denis Packan from ONERA for their help in the experimental work as well as Matthieu Garcia and Ulysse Weller from CNES for the insightful discussions. This research was supported by CNES and ONERA thanks to a Ph.D. allowance granted to Romain Pioch and to the CNES (Grant No. 220835).

AUTHOR DECLARATIONS

Conflict of Interest

The authors have no conflicts to disclose.

Author Contributions

Romain Pioch: Conceptualization (equal); Data curation (equal); Formal analysis (equal); Investigation (equal); Methodology (equal); Validation (equal); Visualization (equal); Writing – original draft (equal); Writing – review & editing (equal). **Victor Desangles:** Conceptualization (equal); Data curation (equal); Formal analysis (equal); Funding acquisition (equal); Investigation (equal); Methodology (equal); Project administration (equal); Supervision (equal); Validation (equal); Visualization (equal); Writing – original draft (equal); Writing – review & editing (equal). **Pascal Chabert:** Conceptualization (equal); Formal analysis (supporting); Investigation (supporting); Methodology (supporting); Project administration (equal); Supervision (lead); Validation (supporting); Writing – review & editing (supporting).

DATA AVAILABILITY

The data that support the findings of this study are available from the corresponding author upon reasonable request.

APPENDIX: COMPUTATION OF THE THRUST CORRECTION FACTORS

1. Multiple charged species

To assess the influence of the presence of multiple charged ions on the indirect thrust, we consider a plasma composed of singly charged ions of density n_I, velocity v_I, and energy E_I and doubly charged ions of density n_{II}, velocity v_{II}, and energy E_{II}. We introduce the parameter η such that $n_{II} = \eta n_I$. The ion energies of these two populations are considered equals,

$$E_I = E_{II} \Rightarrow \frac{m_i}{2e} v_I^2 = \frac{m_i}{4e} v_{II}^2$$
$$\Rightarrow v_{II} = \sqrt{2} v_I.$$

On the one hand, the thrust estimated from the Faraday cup measurements is

$$T^{\text{mes}} = \pi \rho^2 \frac{m_i v_I}{e} \int_{-\frac{\pi}{2}}^{\frac{\pi}{2}} (e n_I v_I + 2 e n_{II} v_{II}) \cos(\theta) |\sin(\theta)| \mathrm{d}\theta$$
$$= \left(1 + 2\sqrt{2}\eta\right) T_I,$$

where T_I is the contribution of the singly charged ions to the thrust.

On the other hand, the total thrust, measured with the thrust stand, is the sum of the contribution of the singly and doubly charged ions such that

$$T^{\text{tot}} = T_I + T_{II}$$
$$= (1 + 2\eta) T_I.$$

The correction factor, defined as the ratio of T^{mes} and T^{tot} is then expressed as

$$K_{\text{multi}} = \frac{1 + 2\sqrt{2}\eta}{1 + 2\eta}.$$

2. Charge exchange collisions

To assess the contribution of charge exchange collisions to the indirect thrust, we consider that some ions have encountered a charge exchange collision during their acceleration in the magnetic nozzle of the ECR thruster. These collisions result in a population of slow ions, of density $n_{i,s}$ and energy $E_{i,s}$, and in a population of fast neutrals of density $n_{n,f}$ in addition to the main (and fast) population of ions of density $n_{i,f}$ and energy $E_{i,f}$. We introduce the parameters τ and κ, such as $n_{i,s} = \tau n_{i,f}$ and $E_{i,s} = \kappa E_{i,f}$. The fact that every charge exchange collision results in one fast neutral per slow ion is given as

$$n_{n,f} = n_{i,s}.$$

Moreover, the energy of a fast neutral depends on the energy of the ion before its collision with a slow neutral. The energy gain in the magnetic nozzle of the slow ions is $E_{i,s}$, therefore, the energy of the fast neutrals is $E_{i,f} - E_{i,s}$. We then have

$$\begin{cases} n_{n,f} = n_{i,s} = \tau n_{i,f}, \\ E_{n,f} = E_{i,f} - E_{i,s} = (1 - \kappa) E_{i,f}. \end{cases}$$

On the one hand, the thrust estimated from Faraday cup measurements takes into account the contribution of slow ions resulting from a charge exchange collision only in the ion current density measurement. The ion velocity term in Eq. (5) captures only the energy of the fast ions. The thrust measured is then expressed as

$$T^{\text{mes}} = \pi \rho^2 \frac{m_i v_{i,f}}{e} \int_{-\frac{\pi}{2}}^{\frac{\pi}{2}} e(n_{i,s} v_{i,s} + n_{i,f} v_{i,f}) \cos(\theta) |\sin(\theta)| \mathrm{d}\theta$$
$$= \left(1 + \tau\sqrt{\kappa}\right) T_{i,f},$$

where $T_{i,f}$ is the contribution of the fast ions to the thrust.

On the other hand, the total thrust measured with the thrust stand, T^{tot}, is the sum of the contributions of the fast ions, slow ions, and fast neutrals to the thrust, respectively, $T_{i,f}$, $T_{i,s}$, and $T_{n,f}$, such that

$$T^{\text{tot}} = T_{i,f} + T_{i,s} + T_{n,f}$$
$$= (1 + \tau\kappa + \tau(1 - \kappa)) T_{i,f}$$
$$= (1 + \tau) T_{i,f}.$$

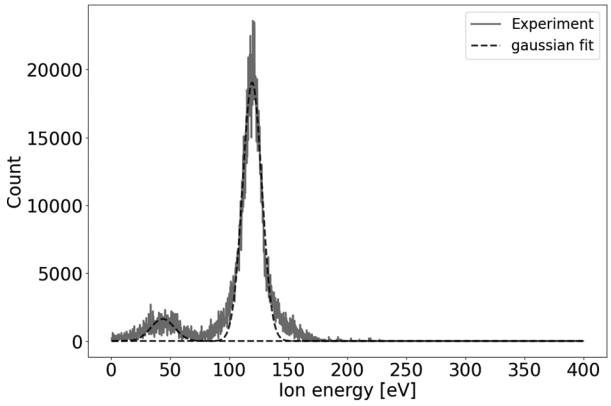

(a)

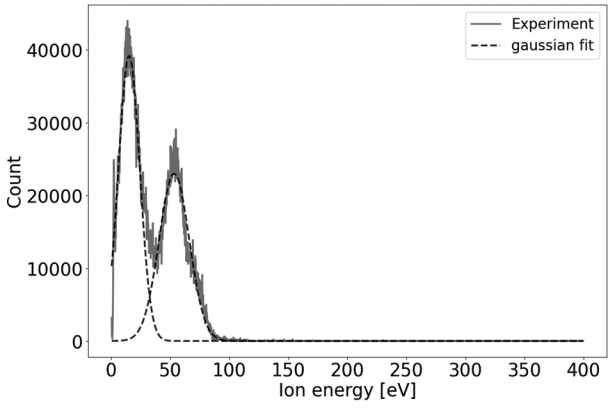

(b)

FIG. 18. Ion energy scan performed in the plume of the ECR thruster for (a) 1.6 sccm and (b) 2.4 sccm for a thruster power of 30 W.

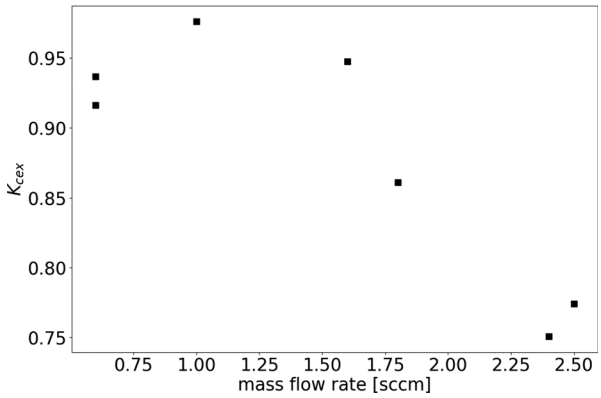

FIG. 19. Evolution of the correction factor K_{cex} with the mass flow rate for a thruster power of 30 W.

The correction factor defined as the ratio of T^{mes} and T^{tot} is then given as

$$K_{cex} = \frac{1 + \tau\sqrt{\kappa}}{1 + \tau}.$$

Figures 18(a) and 18(b) show measurements performed with an ion analyzer for two different mass flow rates. For each signal, two peaks are observed, the high- and low-energy peaks correspond to the fast and slow ions population, respectively. The factors τ and κ are measured as the ratio between the integral of the two peaks and the ratio between the average energy of the two peaks, respectively. To simplify the calculations, signals are fitted with the sum of two Gaussian functions. Figures 18(a) and 18(b) demonstrate the evolution of the relative populations of fast and slow ions with the mass flow rate. The slow ion population becomes dominant at 2.4 sccm.

The evolution of K_{cex} with the thruster mass flow rate is shown in Fig. 19. Two things are to be considered to distinguish the influence of the slow ions and the fast neutrals on K_{cex}. First, it is clear from the above-mentioned equations that $T^{mes} > T_{i,f} + T_{i,s}$. This is due to the assumptions made in Sec. IV B, where the ion velocity is taken only from the energy of the fast ions. Second, Fig. 19 shows that $T^{mes} < T^{tot} = T_{i,f} + T_{i,s} + T_{n,f}$. This result shows that not taking into account the fast neutrals induces an underestimation of T^{mes} that is significantly greater than the overestimation induced by the presence of slow ions.

Ionization outside the source of the thruster could also account for the presence of a low-energy peak in the ion analyzer signals. However, this phenomenon is discarded in this analysis because the frequency of ionization is smaller than the frequency of charge exchange collisions.

REFERENCES

[1]E. Y. Choueiri, "A critical history of electric propulsion: The first 50 years (1906–1956)," J. Propul. Power **20**, 193–203 (2004).
[2]S. Mazouffre, "Electric propulsion for satellites and spacecraft: Established technologies and novel approaches," Plasma Sources Sci. Technol. **25**, 033002 (2016).
[3]C. S. Olsen, M. G. Ballenger, M. D. Carter, F. R. C. Díaz, M. Giambusso, T. W. Glover, A. V. Ilin, J. P. Squire, B. W. Longmier, E. A. Bering, and P. A. Cloutier, "Investigation of plasma detachment from a magnetic nozzle in the plume of the vx-200 magnetoplasma thruster," IEEE Trans. Plasma Sci. **43**, 252–268 (2015).
[4]K. Takahashi, "Magnetic nozzle radiofrequency plasma thruster approaching twenty percent thruster efficiency," Sci. Rep. **11**, 2768 (2021).
[5]V. Désangles, D. Packan, J. Jarrige, S. Peterschmitt, P. Dietz, S. Scharmann, K. Holste, and P. J. Klar, "Ecra thruster advances: 30w and 200w prototypes latest performances," J. Electric Propul. **2**, 10 (2023).
[6]D. M. Goebbel and I. Katz, *Fundamentals of Electric Propulsion: Ion and Hall Thrusters* (Wiley, 2008).
[7]J. Jarrige, P. Thobois, C. Blanchard, P.-Q. Elias, D. Packan, L. Fallerini, and G. Noci, "Thrust measurements of the gaia mission flight-model cold gas thrusters," J. Propul. Power **30**, 934–943 (2014).
[8]D. L. Brown, M. L. R. Walker, J. Szabo, W. Huang, and J. E. Foster, "Recommended practice for use of faraday probes in electric propulsion testing," J. Propul. Power **33**, 582–613 (2017).
[9]S. Mazouffre and G. Largeau, "Evaluation of various probe designs for measuring the ion current density in a hall thruster plume," in *35th International Electric Propulsion Conference* (Electric Rocket Propulsion Society, 2017).
[10]V. Hugonnaud, "Plasma probe measurements for electric propulsion device ion beam: Optimization and standardization," Ph.D. dissertation (Technischen Universität Wien, 2022).
[11]V. Hugonnaud, S. Mazouffre, and D. Krejci, "Faraday cup sizing for electric propulsion ion beam study: Case of a field-emission-electric propulsion thruster," Rev. Sci. Instrum. **92**, 084502 (2021).
[12]V. Hugonnaud, D. Krejci, S. Mazouffre, S. Zoehrer, E. Bosch Borràs, and N. Wallace, "Study of Faraday cup designs suiting multiple electric propulsion systems," in *37th International Electric Propulsion Conference* (Electric Rocket Propulsion Society, Cambridge, 2022).
[13]M. R. Inchingolo, M. Merino, and J. Navarro-Cavallé, "Plume characterization of a waveguide ECR thruster," J. Appl. Phys. **133**, 113304 (2023).
[14]J. Benedikt, H. Kersten, and A. Piel, "Foundations of measurement of electrons, ions and species fluxes toward surfaces in low-temperature plasmas," Plasma Sources Sci. Technol. **30**, 033001 (2021).
[15]J. D. Johnson and A. J. T. Holmes, "Edge effect correction for small planar Langmuir probes," Rev. Sci. Instrum. **61**, 2628–2631 (1990).
[16]R. Hofer, M. Walker, and A. Gallimore, "A comparison of nude and collimated faraday probes for use with hall thrusters," in *27th International Electric Propulsion Conference* (Electric Rocket Propulsion Society, Fairview Park, OH, 2001), pp. 15–19.
[17]N. S. Mühlich, J. Gerger, B. Seifert, and F. Aumayr, "Simultaneously measured direct and indirect thrust of a FEEP thruster using novel thrust balance and beam diagnostics," Acta Astronaut. **197**, 107–114 (2022).
[18]S. Peterschmitt, "Development of a stable and efficient electron cyclotron resonance thruster with magnetic nozzle," Ph.D. dissertation (Institut Polytechnique de Paris, 2022).
[19]T. Vialis, J. Jarrige, A. Aanesland, and D. Packan, "Direct thrust measurement of an electron cyclotron resonance plasma thruster," J. Propul. Power **34**, 1323–1333 (2018).
[20]F. Cannat, "Caractérisation et modélisation d'un propulseur plasma à résonnance cyclotronique des électrons," Ph.D. dissertation (Ecole Polytechnique, 2015).
[21]T. Vialis, "Développement d'un porpulseur plasma résonance cyclotron électronique pour les satellites," Ph.D. dissertation (Sorbonne Université, 2018).
[22]F. Boni, "Development of a microwave plasma diagnostic applied to electric propulsion systems," Ph.D. dissertation (Université Paris Saclay, 2022).
[23]R. Gueroult, "Etude d'une source d'ions obtenue par extraction et accéléération d'ions à partir d'une source plasma filaire," Ph.D. dissertation (Ecole Polytechnique, 2011).
[24]D. A. Dahl, "simion for the personal computer in reflection," Int. J. Mass Spectrom. **200**, 3–25 (2000).
[25]H. D. Hagstrum, "Auger ejection of electrons from molybdenum by noble gas ions," Phys. Rev. **104**, 672–683 (1956).

[26]J. Williams, M. Johnson, and D. Williams, "Differential sputtering behavior of pyrolytic graphite and carbon-carbon composite under xenon bombardment," AIAA Paper No. 2004-3788, 2004.
[27]J. S. Miller, S. H. Pullins, D. J. Levandier, Y.-H. Chiu, and R. A. Dressler, "Xenon charge exchange cross sections for electrostatic thruster models," J. Appl. Phys. **91**, 984–991 (2002).
[28]J. C. Sercel, "An experimental and theoretical study of the ECR plasma engine," Ph.D. dissertation (Californa Institute of Technology, 1993).
[29]E. B. Hooper, "Plasma detachment from a magnetic nozzle," J. Propul. Power **9**, 757–763 (1993).
[30]E. Ahedo and M. Merino, "On plasma detachment in propulsive magnetic nozzles," Phys. Plasmas **18**, 053504 (2011).